Ceramic to metal direct brazing

F. Moret, N. Eustathopoulos

JOURNAL DE PHYSIQUE IV
Colloque C7, supplément au Journal de Physique III, Volume 3, novembre 1993

Ceramic to metal direct brazing

F. MORET and N. EUSTATHOPOULOS*

CEREM/Laboratoire de Génie des Matériaux, CENG, 85X, 38041 Grenoble cedex, France
** INPG/LTPCM, ENSEEG, BP. 75, 38402 Saint Martin d'Hères, France*

The production of important components like first walls of thermonuclear power reactors, advanced automotive or aeronautic turbines and heat exchangers depends on the control of ceramic to metal joining techniques, especially direct brazing. Recent advances in two fundamental aspects of such techniques are reviewed: thermodynamics and mechanics. About thermodynamics, a general theory of wetting and adhesion of active filler alloys on oxide ceramics is described. This approach allows the determination of optimal braze compositions. Some of the concepts of this approach are used for non oxide ceramics. Due to a complex stress field existing in the ceramic at the location of crack initiation and propagation, accurate failure prediction of ceramic to metal assemblies remains a challenge. Nevertheless, simple analytical calculations are often a useful tool. For more advanced analysis, determination of joint constitutive laws by inverse method and careful finite element enmeshment in the vicinity of the joint allow accurate stress field calculations.

INTRODUCTION

Depending on the composition, the valuable properties of ceramics are temperature, corrosion, wear and erosion resistance, insulating, biochemical, dielectric, magnetic and superconducting properties. Recently developed materials like particulate or fiber reinforced glass and ceramic matrix composites are extending this application field. But joining ceramics to other ceramic or metallic materials often remains an unresolved or unsatisfactorily resolved problem. Today, ceramic joining is one of the key technologies for the use of ceramic materials in industry. Numerous R&D are carried out in that field [1, 2, 3].

Among the various bonding techniques (mechanical, adhesive, solid state), brazing offers high joint strength (close or equal to that of the ceramic), high in service temperature (about 0.6 the absolute melting temperature of the braze), excellent thermal and electrical conductivity, excellent tighness and moderate costs. Due to the general non wetting of commercial filler metals to ceramics, metallisation of the ceramic surface (Mo-Mn paste, hydride PVD coating) followed by a reaction thermal treatment are often used.

Direct or active brazing has been developed to simplify the manufacturing of brazed ceramic joints: the filler metal contains an active element (like Ti, Zr, ...) which promotes a good wetting of the ceramic surface and eliminates the need for metallisation treatments. As reactive elements are avid of oxygen, active brazing is conducted in vacuum furnaces ($<10^{-5}$ mbar).

After a short chapter on applications of ceramic brazing, the two main aspects of this technique, thermodynamics and mechanics, will be presented. In this brief overview, we won't detail non destructive evaluation and other technologies involved in the manufacturing of ceramic to metal assemblies, despite their strong importance at the industrial scale.

APPLICATIONS

Ceramic to metal direct brazing is used to manufacture the plasma facing components of thermonuclear fusion reactors (see [4] for example). Carbon base refractory tiles (graphite, C-C composite) are brazed onto cooled TZM, steel or copper structures. In electrical engineering, alumina parts are brazed in insulators and tight connectors. Brazing of aluminum nitride is developed for the production of power electronic components.

Due to its high thermal conductivity, good thermal shock behaviour and excellent corrosion resistance, silicon carbide has a potential market in heat exchangers for the high temperature range in aeronautical, automotive and power generation

industries, and for the medium temperature range in chemical industry. Significant research effort is today devoted to find out brazing techniques suitable for such applications. In the french-swedish AGATA program, wheel/shaft joining of silicon nitride turbines for hybrid electrical vehicles needs direct brazing technologies.

Mechanical parts as tools and sleeves are reinforced by brazed alumina or silicon nitride wear resistant tiles. Aeronautical turbines include ceramic abradables and the use of structural bulk ceramics and ceramic-ceramic composites is in project for components like vanes, blades, blisks and exhaust parts.

THERMODYNAMICS OF REACTIVE BRAZING

Introduction

To establish chemical bonds between ceramics and substrates is the first general difficulty to which joining technologies are faced. A too strong chemical reactivity between the ceramic and the substrate can lead to interfacial degradation and fracture during the in service life, due to the generally high temperatures involved. Interfacial compounds with carefully adjusted properties are to be used. Using material data bases and sessile drop experiments, thermodynamical calculations are predicting the phase transformations occuring at the interface and allow the optimization of interlayer and filler metals. This methodology will now be emphasized in the case of oxide ceramics brazing.

Wetting

In pure reactive metal/oxyde systems, the oxydo-reduction reaction is generally used to discuss reactivity [5,6]. We will focus on the case of the reduction of alumina by a metal M with the formation of a MO oxide, according to the following reaction:

$$\frac{3}{2}(M)+\frac{1}{2}Al_2O_3 \leftrightarrow \frac{3}{2}MO+(Al) \qquad (1)$$

The degree of progress of the interfacial reaction (1) can be obtained by calculating the equilibrium concentration of Al in liquid M, coming from the dissolution of Al_2O_3. This degree of progress is equal to the difference between final and initial (that is zero in our case) mole fraction of Al, X_{Al}. In the case where $X_{Al} << 1$, the equilibrium X_{Al} for reaction (1) is written as follows:

$$X_{Al} = \exp-\left(\frac{\Delta G_R^*}{R.T}\right) \qquad (2)$$

As will be seen further, the term $\Delta G_R^* / R.T$ is used to establish a rough scale of relative reactivity for different systems.

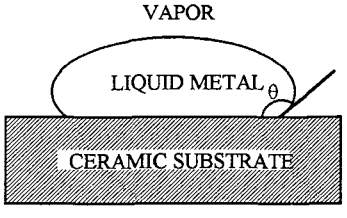

Figure 1: Definition of the contact angle θ of a liquid on a flat surface.

There is at the present time no theory of general acceptance capable of describing satisfactorily reactive wetting, e.g. wetting followed by material transfert at the solid-liquid interface. According to LAURENT [7], the smallest contact angle (as defined in figure 1) possible in a reactive system is given by:

$$\cos\theta_{min} = \cos\theta_0 - \frac{\Delta\sigma_r}{\sigma_{LV}} - \frac{\Delta G_r}{\sigma_{LV}} \qquad (3)$$

where θ_0 is the contact angle of the liquid on the substrate in the absence of any reaction and σ_{LV} is the interfacial energy between the liquid and the vapor phase. $\Delta\sigma_r$ takes into account the change in interfacial energies brought by the interfacial reaction. ΔG_r is the change in free energy per unit area, released by the reaction of the material contained in the "immediate vicinity of the metal-substrate interface" [8].

At least for systems with weak or moderate reactivity, the governing parameter of reactive wetting appears to be the term reflecting interfacial energy change $\Delta\sigma_r$, rather than the transient Gibbs free energy term ΔG_r [9]. However, the importance -and even the predominance- of this last term must not be excluded in some cases, for instance when an intense reaction strongly localized at the triple line occurs.

Practically, pure metal-oxyde systems can be divided in three categories:

1) In systems for which $\Delta G_R^* / R.T >> 0$ (typically greater than 20), the contact angle $\theta \approx 120°$. Weak physical (Van der Waals) and interface chemical metal-oxide bonds are localized at the sharp interface [5,10,11,12,13].

2) If $\Delta G_R^* / R.T \approx 10$, an improvement of wetting is obtained with regard to the preceding case ($\theta \approx 80°$), due to the effect of adsorbed oxygen at the interface, produced by the dissolution of the oxide substrate. This effect is greatly enhanced by the formation of metal-oxygen clusters.

3) When $\Delta G_R^* / R.T \leq 0$, both dissolution of the oxide substrate and precipitation of a new phase occur. Wetting will depend on the nature of the interfacial layer: for iono-covalent compounds, a case 2) behaviour will be observed whereas for metallic compounds (metallic-like oxides or intermetallics), nearly perfect wetting can be expected.

A strong improvement of wetting of a non-reactive metal can be obtained adding a solute B, like titanium, that leads to an in-situ modification of both liquid and solid sides of the interface. Such an improvement will be possible if this solute develops strong solute-solute interactions with dissolved oxygen. Two cases have to be considered, depending on the value of the Wagner's first order interaction parameter ε_O^B which characterizes the strength of the interaction between the solute B and dissolved oxygen O (the more highly negative ε_O^B is, the stronger the B-O interaction is):

a) If $\varepsilon_O^B < 0$, an adsorption layer rich in reactive element B and oxygen is formed at the liquid side;

b) If $\varepsilon_O^B << 0$, a new phase precipitates at the interface. If this new precipitation is continuous along the interface and if its bonding character is at least partially metallic, the wetting is strongly improved.

As the Ti-O interaction is strong, titanium is often chosen as solute element in filler metals to improve the wetting on alumina and other oxide ceramics.

Adding Ti to NiPd alloys placed on alumina substrates, a series of wetting transitions is observed at particular values of X_{Ti}^*, due to a change in the type of the Ti oxide precipitated at the interface [14].

Adhesion

As for wetting, braze-ceramic adhesion and mechanical strength depend on the metallic character of the oxide precipitated at the interface. The example of the PdCu-Ti/alumina system is similar to the NiPd-Ti/alumina one. The nature of the oxide depends on the Ti content of the braze (table 1).

Ti content of the braze (%)	Contact angle θ (°)	Work of adhesion W (mJ/m2)	Interfacial oxide	Conduction type of interfacial oxide	Fracture type
0	127	560	Al_2O_3	Insulator	Adhesive
4	92	1350	$Ti_4O_7 (Ti_3O_5)$	Semi-metallic	Adhesive
7	70	1880	Ti_2O_3	Semi-metallic	Adhesive
24.7	18	2730	$TiO_{1.2\pm0.04}$	Metallic	Cohesive

Table 1: Wettability, work of adhesion, interfacial chemistry and fracture type of CuPd-Ti/alumina sessile drop specimens. The fracture type (see figure 2 for definition) is correlated with the metallic character of the oxide precipitated at the interface. From [15].

Metallic character and low thickness of the interfacial oxide are associated with high strength interfaces (cohesive fracture, see figure 2). When broken using more sophisticated mechanical tests (tensile, shear), cohesive fracture interfaces exhibits stresses to failure close or equal to the one of bulk ceramic material.

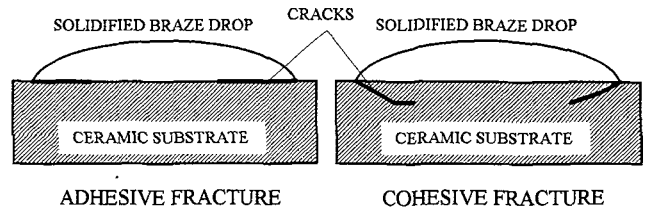

Figure 2: Definitions of adhesive and cohesive fracture types.

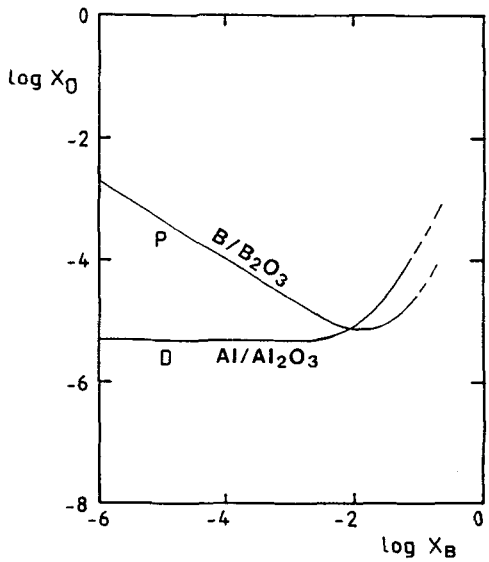

Figure 3: Thermodynamics of braze (matrix A-active solute B) on alumina system (ε_O^B<0). Log-log diagram of equilibrium mole fraction of oxygen as a function of solute B composition for the dissolution of alumina by the braze (curve D) and the precipitation of a B oxide (curve P). In that case corresponding to A=Ni and B=Ti at 1773K, the solute B reduces alumina on the right of the intersection point of the two curves [16,17].

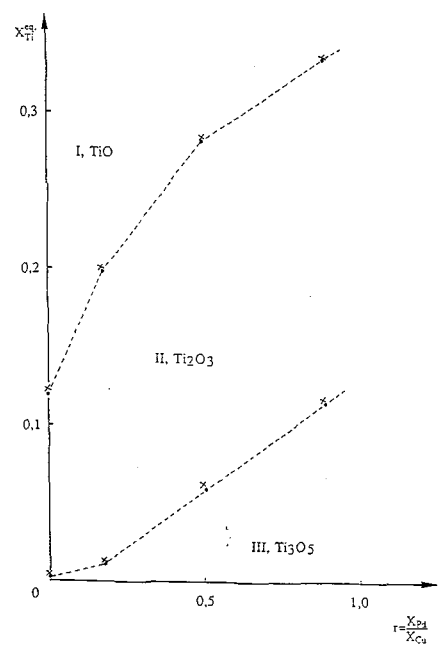

Figure 4: Calculated map of precipitating oxides for the PdCu-Ti braze/alumina system. The mechanical strength of the joint is close to the fracture strength of bulk alumina when the TiO oxide (metallic character) is formed. Pd, Cu and Ti compositions are adjusted to obtain this condition. From [15].

New braze formulations

The development of new braze formulations are based on these experimental observations. In practice, to exploit interfacial reactions between the metal and the ceramic, one can alloy a non reactive base alloy (A: Ag-Cu, Pd-Cu, Pd-Ni, Ni-Fe-Cr, etc...) with controlled quantities of reactive solute (B) additions (Ti, Zr, etc...), leading to the optimum relation between wettability and reactivity. Thermodynamic calculations help to determine optimum formulations.

The chemical interactions in the A-B/alumina system can be described by the dissolution of alumina in the alloy possibly followed by the precipitation of a B oxide at the interface (for example B_2O_3):

$$Al_2O_3 \leftrightarrow 2(Al) + 3(O) \quad (4)$$

$$2(B) + 3(O) \leftrightarrow B_2O_3 \quad (5)$$

Assuming small values of the mole fractions of B and Al and for each B solute concentration, the equilibrium mole fraction of dissolved oxygen in the braze, X_O, can be calculated [9] (figure 3) for the dissolution reaction (4) (curve D, X_O^D) and the precipitation reaction (5) (curve P, X_O^P). If for the same value of the solute concentration X_B, the inequality $X_O^D > X_O^P$ is verified (case of figure 3), the solute B will reduce the alumina, forming B_2O_3:

$$Al_2O_3 + 2(B) \leftrightarrow B_2O_3 + 2(Al) \quad (6)$$

These calculations can be reproduced for each possible oxide B_xO_y and maps of precipitating oxide types can be established (figure 4).

Non-oxide ceramics

Although all the examples are concerning oxide substrates, some of these concepts can be applied to other kind of ceramics, including carbides and nitrides. For example, the contact angle of copper on a covalent carbide such as B_4C is very high (136° [5]), while it is only a few tens of degrees on metallic like carbides such as chromium or molybdenum carbides [5]. However, metallicity and reactivity are not the only criteria for a good wettability and mechanical strength of metallic brazes on non-oxide ceramics. Indeed, a good wetting is observed for some metals on covalent ceramics. For instance, liquid Al is wetting TiN [18] and liquid Si is wetting SiC [5,19].

For such applications for which no commercial filler metal exists, radically new braze compositions have been developed and tested. Good wetting, cohesive fracture with stress to failure equal to that of bulk ceramic and excellent corrosion resistance have been demonstrated [20] (figure 5).

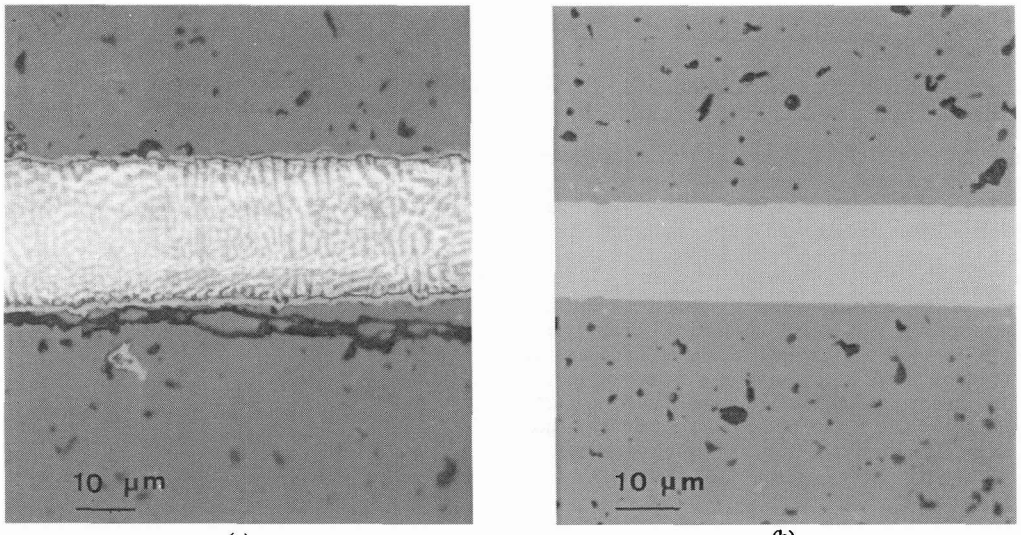

(a) (b)

Figure 5: SiC to SiC brazing using (a) a commercial AgCu-Ti filler metal and (b) a radically new braze composition. Cracks and porosities due to the uncontrolled reactivity in (a) are totally eliminated in (b). The fracture stress is equal to that of bulk SiC [20].

MECHANICS OF BRAZED JOINTS

Introduction

Thermal expansion mismatch between ceramics and most of the other materials is the second general difficulty to obtain performant and reliable asssemblies. The low thermal expansion and generally high Young modulus of ceramics induces very high stresses during the manufacturing and the life of the heterogeneous assemblies. If no special care is taken, these stresses lead to ceramic fracture due to the low ceramic toughness. Special geometries and interfacial layers with adapted mechanical and expansion properties are needed to avoid premature failures. Numerical mechanical calculations are a fruitful tool to shorten the development delay and insure the attainment of the life time objectives.

The first step of the approach is the calculation of the stress field. The main parameters will first be described through a heuristic approach. Then, problems arising from joint constitutive law determination and numerical analysis will be emphasized. Fracture and damage prediction from this stress field will then be discussed.

Heuristic approach

A simple elastic analytical approach gives a first order of magnitude of the longitudinal stress at the joint interface in a ceramic part, for example alumina (mark 1), bonded to a steel substrate (mark 2):

$$\sigma_1 = E_1.\phi.\int_{T_0}^{T}(\alpha_1-\alpha_2).dT \qquad (7)$$

E_i are the Young modules, α_i are the coefficients of thermal expansion (CTE) and ϕ is a geometrical factor equal to $(1+S_1.E_1/S_2.E_2)^{-1}$ for a plane geometry without bending and neglecting the joint. S_i are the sections of the materials. Other parameters are T_h, the "hardening" temperature of the joint, and T_0, the final room temperature. Assuming that both materials have the same width but different thicknesses h_i and a constant CTE versus temperature, (7) becomes:

$$\sigma_1 = \frac{1}{1+\frac{h_1}{h_2}.\frac{E_1}{E_2}}.E_1.\Delta\alpha.\Delta T \qquad \text{with} \quad \Delta\alpha = \alpha_1-\alpha_2 \quad \text{and} \quad \Delta T = T_h - T_0 \qquad (8)$$

20°C	α (K^{-1})	E (GPa)	σ_y (MPa)
Alumina	$8.6.10^{-6}$	310	180
Steel	12.10^{-6}	200	500

Table 2: Typical material properties of alumina and a martensitic steel at 20°C.

Equation (8) and CTE values in table 2 are showing that the interfacial stress in the alumina is compressive. No fracture can occure at this location. As shown in figure 6, if $h_1=h_2=h$, $E_1=E_2=E$, then the neutral fiber will be located in the middle of each material and a tensile stress also given by (8) is experienced on the surface of the ceramic. Fracture may then occure if this stress is higher than the yield stress of the ceramic given in table 2.

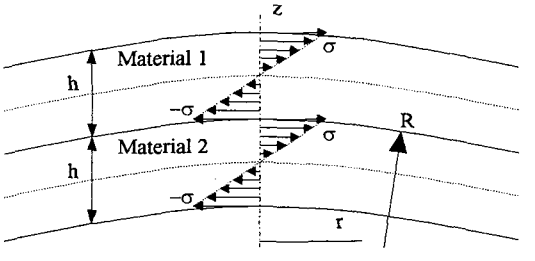

Figure 6: σ_{rr} stress distribution in a typical axisymmetrical ceramic (material 1) to metal (material 2) joining when $h_1=h_2=h$, $E_1=E_2=E$ and assuming elastic deformations. As a compressive stress state exists in the ceramic at the interface, a corresponding tensile stress of same magnitude is experienced on the surface of the ceramic and may induce the fracture. This stress state creates a bending of radius R.

The order of magnitude of the residual tensile stress at room temperature on the surface of an alumina part bonded to a martensitic steel part (relatively low expansion steel grade) of same width is given in table 3 for three values of the thickness ratio and two bonding techniques.

Table 3: Order of magnitude of the residual tensile stress on the surface of a plane alumina part bonded to a martensitic steel part using two joining techniques. Stress values are calculated using equation (8) and material data in table 2.

Thickness ratio $h_{Alumina}/h_{Steel}$	Brazing with an AgCu based filler metal $T_b = 0.6.T_m$	Solid state bonding at 1200°C
	ΔT = 297 K	ΔT = 1180 K
10 (compliant steel plate)	19 MPa (no fracture)	75 MPa (no fracture)
1 (partly stiff steel plate)	123 MPa (?)	488 MPa (fracture)
0,01 (fully stiff steel plate)	308 MPa (fracture)	1225 MPa (fracture)

Two remarks must be carried out:

.The stress does not depends on the length of the joint. On the contrary, experiments show that for sufficiently small joint length (several millimeters), no fracture is observed even with high stresses. This apparent discrepancy is explained by fracture mechanics and will be detailed later: for small joint length, the stored elastic energy is not sufficient to initiate a fracture.

.When the stress is higher than the steel yield stress (table 2), plasticity of steel decreases the stresses approximately down to the yield stress.

Comparison of calculated stresses with fracture strength of alumina shows that joining is possible by every technique where the steel foil is thin, only brazing may allow joining when both thicknesses are close and no technique is available when the steel substrate is stiff. In this later case, other substrate materials with adapted CTE must be used (titanium or controled CTE iron or nickel grades).

Stress field calculation

Such simple calculations gives useful orders of magnitude for some of the parameters of the assembly. But various phenomenons (bending, edge effects, localisation, plasticity, fracture mechanics) are not considered and strongly modify the value of the stress to be taken into account in the failure analysis.

The first phenomenon to be considered is the bending of the sample. Considering a flat specimen made of two brazed plates, a camber is observed after cooling down. This deformation can be calculated assuming an elastic behaviour of materials in the axisymmetric shell assumption. The z axis displacement u_Z obeys a spherical law of radius R [21,22] and the resulting theoretical camber U of a specimen of radius r is given by:

$$U = \frac{r^2}{2.R} \qquad \text{with} \qquad \frac{1}{R} = \frac{1}{H}\cdot\frac{6.(1+\varepsilon).f.(1-f)}{\varepsilon^2.f^4+2.\varepsilon.(2.f^3-3.f^2+2.f)+1}.\Delta\alpha.\Delta T \qquad (9)$$

ε depends on E_i and on the Poisson coefficients ν_i, and f is a geometrical factor:

$$\varepsilon = \frac{\beta_1}{\beta_2} - 1 \qquad \text{with} \quad \beta_i = \frac{E_i}{2.(1-\nu_i)} \quad ; \qquad f = \frac{h_1}{H} \quad \text{with} \quad H = h_1 + h_2 \qquad (10)$$

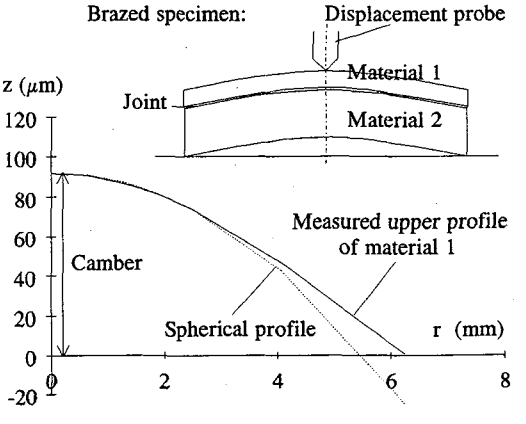

Figure 7: Comparison of measured and theoretical profiles of an axisymmetric brazed specimen (2.7 mm in heigth). Experimental data is from [23]. Model materials are used (material 1 is TZM, a molybdenum alloy, material 2 is A316L stainless steel, filler alloy is InCuSil ABA). As the agreement between experimental and spherical profiles is good up to about half the radius, a strong discrepancy is observed after due to edge effects. The brazed specimen geometry and the definition of the camber (U) and its in-situ measurement by a displacement probe in a vertical dilatometer are illustrated.

Comparison with experimental data shows that even if an uniform curvature is observed in the axis area, the loss of stiffness close to the edges slightly reduces the camber (figure 7). As experimental failures generally occure from the edges, this example demonstrates that analytical calculations are irrelevant for accurate fracture prediction.

Finite element calculations allow the determination of strains and stresses fields in the whole assembly even for complex shapes. The accuracy of the calculations depends primarily upon the accuracy of materials constitutive laws from room temperature up to the joint solidification temperature. As elastic constants are often sufficient for the ceramic, complemental measurements are generally necessary for the metallic substrate especially to identify strain hardening and high temperature creep parameters. The joint constitutive law often remains the less accurately known.

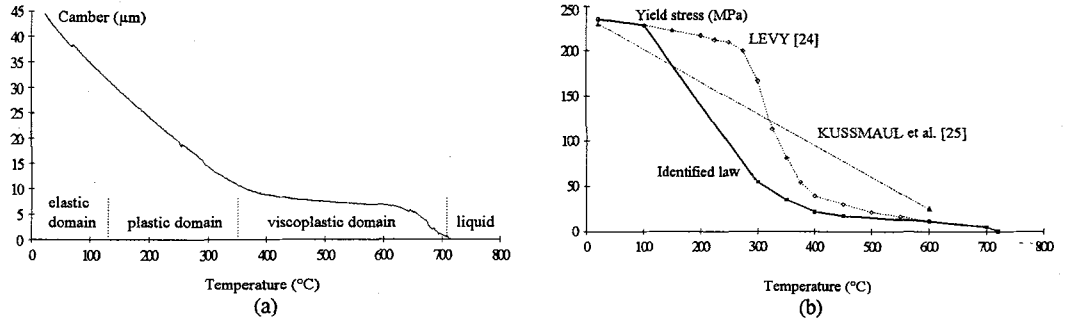

Figure 8: (a) Record of the camber versus temperature during the cooling down after brazing of the TZM/InCuSil ABA/A316L model specimen described in 2. (b) Plastic constitutive law of the joint identified using an inverse method from the camber vs temperature curve. This law is compared with other ones used in litterature for FEM calculations involving InCuSil ABA filler alloy [23].

The joint material is the product of the liquid and solid state reactions between the filler alloy, the ceramic and the substrate. Its coarse solidification microstructure is far different from the fine rolled microstructure of the initial filler alloy foil. Its low thickness (10-100 µm) prohibits classical mechanical tests. Based on the experimental set described in figure 7, an inverse method has been successfully applied to determine this constitutive law [23] (figure 8). Identification of the constitutive law is performed with an optimisation algorithm from iterative finite element calculations based on the specimen enmeshment shown in figure 9.

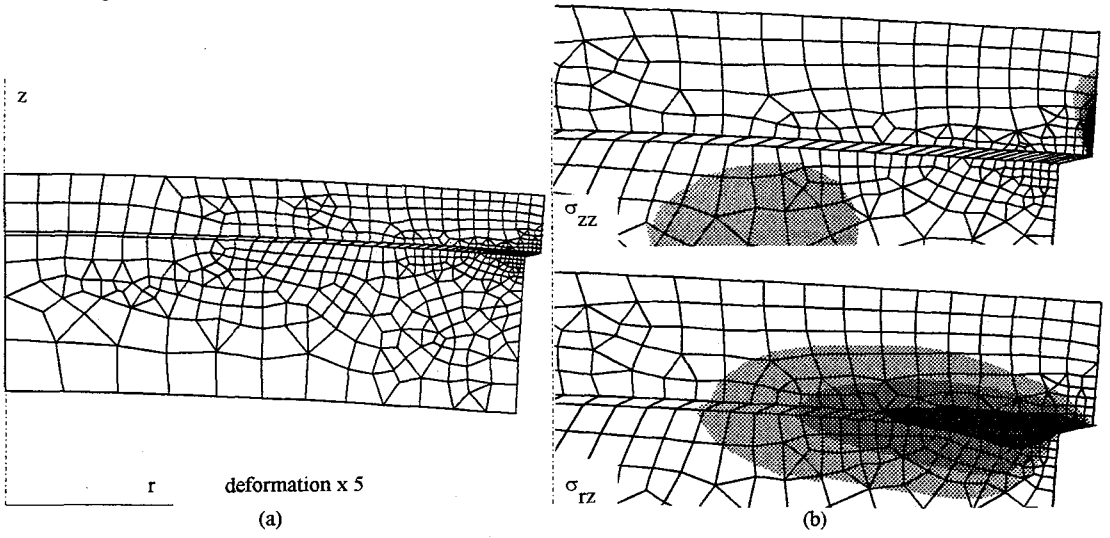

Figure 9: (a) Deformed enmeshment at the end of the cooling down of the TZM/InCuSil ABA/A316L model specimen. (b) Calculated σ_{zz} and σ_{rz} stress fields. A σ_{zz} maximum is observed on the free surface of material 1 just above the joint.

At this step of the modelling work, a good agreement is obtained between calculated and experimental strains and an accurate stress field is available (figure 9 (b)). This stress field is nevertheless not reliable at the joint edge for the following reason.

Along the ceramic-joint interface, finite element calculations are exact because the stress tensor is symmetrical, continuous and bounded, except a tensile stress discontinuity $\Delta\sigma_{rr}$ through the interface (see figure 6):

$$\Delta\sigma_{rr} = E.\Delta\alpha.\Delta T \qquad (11)$$

As can be observed in figure 9 (b), a sharp stress peak is located at the edge of the ceramic-joint interface. This stress concentration is known as the Thorn singularity [26]. The stress and the first partial derivative of stress are unbounded. Consequently, the stress tensor becomes unsymmetrical. As usual finite elements codes are assuming a symmetrical stress tensor, inconsistent stress values are calculated in the two elements closest to the singularity. It is easy to demonstrate that refining the mesh allows an acccurate calculation of stress as close as desired from the interface [27].

Fracture prediction

Fracture modes depends on $\Delta\alpha$ sign and geometry. In the general case depicted by figure 7 example ($\Delta\alpha$ negative), a maximum in tensile stress is observed on the ceramic surface (material 1) above the joint. When the joint is strong enough, mode I crack initiation occurs in the ceramic at this point. The stress becomes compressive soon after but maximum shear stress values are observed. As a consequence, mode I rapidly transforms to mode II crack propagation in the ceramic close and along the joint (figure 10).

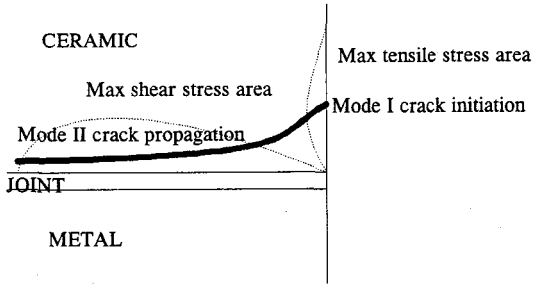

Figure 10: Typical fracture mechanism of a ceramic to metal assembly. If the joint is strong enough, mode I crack initiation occurs on the lateral surface of the ceramic in the maximum tensile stress area and mode II crack propagation follows in the ceramic along the joint in the maximum shear stress area.

Even if such a qualitative description is easy and in good agreement with experimental observations, a quantitative prediction of crack initiation and propagation remains an open problem. The main reasons are:

.The complex stress field prohibits the application of classical fracture mechanics methods and material data based on the assumption of uniform stress far from the crack tip. Simple K_{Ic} criterion cannot apply. The analytical calculations of adapted K_I or K_{II} stress intensity factors as in [28] proved to be uneffective as only comparative informations can be obtained and no plasticity effects can be taken into account.

.G energy releaving factor can only be calculated through complex finite element computations.

This complexity explains that industrial designs of ceramic/metal joints are based on simple criterions like critical values of the maximum calculated main stress (relevant for brittle materials like ceramics).

CONCLUSIONS

The production of important components like first walls of thermonuclear power reactors, advanced automotive or aeronautic turbines and heat exchangers depends on the control of ceramic to metal joining techniques, and especially direct brazing. Recent advances in two fundamental aspects of such techniques have been reviewed: thermodynamics and mechanics.

.About thermodynamics, a general theory of wetting and adhesion of active filler alloys on oxide ceramics has been described. This approach allows the determination of optimal braze compositions. Some of the concepts of this approach have been used for non oxide ceramics.

.Due to a complex stress field existing in the ceramic at the location of crack initiation and propagation, accurate failure prediction of ceramic to metal assemblies remains a challenge. Nevertheless, simple analytical calculations are often a

useful tool. For more advanced analysis, determination of joint constitutive laws by inverse method and careful finite element enmeshment in the vicinity of the joint allow accurate stress field calculations.

ACKNOWLEDGMENTS

The authors acknowledge B. DREVET, P. LE GALLO, G. LOVATO, G. CHAUMAT and J. VALIGNAT for transmission of recent results and their critical comments about this manuscript.

REFERENCES

[1] DOYAMA, M., SOMIYA, S., CHANG, R.P., Eds., "Metal-Ceramic Joints", *Proc. of the MRS Inter. Meeting on Adv. Mater.*, Tokyo, June 2-3 1988, MRS (1989)
[2] KRAFT, W., Ed., "Joining Ceramics, Glass and Metal", *Proc. of the Inter. Conf.*, Bad Nauheim, 1989, DGM (1989)
[3] KRAPPITZ, H., SCHAEFFER, H.A., Eds, "Joining Ceramics, Glass and Metal", *Proc. of the Inter. Conf.*, Königswinter, May 17-19 1993, DGM (1993)
[4] CHAUMAT, G., LEMOINE, P., VALIGNAT, J., *Proc. of the SOFT Inter. Conf.*, Roma (1992)
[5] NAIDICH, J. V., *Prog. Surface Membrane Sci.* **14** (1981) 353
[6] NICHOLAS, M. G., *Joining Ceramic, Glass and Metal*, Ed. W. Kraft, DGM (1989) 3
[7] LAURENT, V., *Thesis*, Grenoble, France (1988)
[8] AKSAY, L.A., HOGE, C.E., PASK, J.A., *J. of Phys. Chem.*, **78** (1974) 1178
[9] EUSTATHOPOULOS, N., DREVET, B., *J. Physique III (F)* (to be published)
[10] TASKER, P.W., STONEHAM, A.M., *J. Chimie Physique*, **84**, 2 (1987) 149
[11] JOHNSON, K.H., PEPPER, S.V., *J. Appl. Phys.*, **53** (1982) 6634
[12] HICTER, P., CHATAIN, D., PASTUREL, A., EUSTATHOPOULOS, N., *J. Chimie Physique*, **85**, 10 (1988) 941
[13] BORDIER, G., NOGUERA, C., *Phys. Review B*, **44**, 12 (1991) 6361
[14] KRITSALIS, P., *Thesis*, Technical University of Athens, Greece (1990)
[15] WAN, C., *Thesis*, Institut National Polytechnique de Grenoble, France (1991)
[16] MERLIN, V, KRITSALIS, P., COUDURIER, L., EUSTATHOPOULOS, N., *Mater. Res. Soc. Symp. Proc.*, **238** (1992) 511
[17] NAIDICH, Y.V., ZHURAVLEV, V.S., CHUPRINA, G., *Sov. Powd. Metall. and Met.. Ceramics*, **13**, 3 (1974) 236
[18] RHEE, S.K., *J. Amer. Ceram. Soc.*, **53** (1970) 386
[19] DREVET, B., KALOGEROPOULOU, S., EUSTATHOPOULOS, N., accepted in *Acta Metall. Mater.*
[20] CEA/CEREM-DEM/LGM, Internal Report (1991)
[21] LE GALLO, P., CEA/CEREM-DEM/LGM, Internal Report (1993)
[22] IANCU, O.T., MUNZ, D., in [2] 257
[23] LOVATO, G., MORET, F., LE GALLO, P., CAILLETAUD, G., PILVIN, P., *Proc. of EUROMAT 93 Conference*, Paris, June 8-10 (1993)
[24] LEVY, A., *J. Am. Ceram. Soc.*, 74 (9) (1991) 2141
[25] KUβMAUL, R., MUNZ, D., in [3] 152
[26] BUI, H.D., TAHERI, S., *C.R. Acad. Sci. Paris*, **309**, II (1989) 1527
[27] WHICOMB, J.D., RAJU, S.J., GOREE, J.G., *Comput. Struct.*, **15**, 1 (1982) 23
[28] SUGA, T., MIZUNO, K., MIYAZAWA, K., in [1] 137